Rev. Adv. Mater. Sci. 57 (2018) 175-182

STRUCTURAL ORGANIZATION OF THE MAGNETIC PART OF SMART MATERIAL BASED ON NANOPARTICLES OF IRON OR MAGNETITE IN PORES OF MCM-41 MESOPOROUS SILICA FOR TARGET DRUG DELIVERY

E.G.Zemtsova, A.N. Ponomareva, A.Y. Arbenin and V.M. Smirnov

St. Petersburg State University, Institute of Chemistry, Universitetskiy pr., 26, St. Petersburg, 198504, Russia

Received: April 25, 2018

Abstract. The important stage of the development of smart material for the target drug delivery is the construction of the magnetic part of this material, including mesoporous silica and magnetic nanoparticles (Fe_3O_4 or Fe^0). Such a system will allow carry out magnetic decapsulation (excretion) of drug from smart material using the magnetic field of a given value in the right place of the body. The paper considers the features of synthesis mesoporous silica MCM-41 with various pore diameter (33-51 Å) and synthesis of superparamagnetic nanoparticles of magnetite or metallic iron in the pores of mesoporous silica. The dependence of magnetic properties of nanocomposites MCM-41/Fe^0 and MCM-41/Fe_3O_4 from the pore diameters of MCM-41 templates is studied. It was found that the matrix has a decisive influence on the content of iron or magnetite nanoparticles. The saturation magnetization of the material increases with increasing pore size of the mesoporous matrix. Nanocomposites MCM-41/Fe^0 and MCM-41/Fe_3O_4 exhibit superparamagnetism, that allows them to be used as a magnetic material for targeted drug delivery.

1. INTRODUCTION

Currently, there is a growing interest in the chemical design of new materials, including ones produced by the structural organization of complex systems [1,2]. This also applies to the creation of more effective biomaterials (i.e. smart materials) with improved functional properties for targeted drug delivery [3,4]. Smart materials are the materials that demonstrate one or several increased physical properties (optical, magnetic, electric, mechanical) under external actions: pressure, temperature, humidity, electric or magnetic fields etc. [3,4]. As noted in the review [5], the number of articles devoted to the creation of complex structured materials with magnetic properties for the diagnosis and creation of targeted drug delivery systems is continuously growing.

Recently, a number of scientific groups have developed systems for targeted delivery of anticancer drugs with the goal to increase the selectivity of chemical therapy. However, there are some problems on this way:

1) The drug should be delivered exclusively to the tumor. The most often technique is the inclusion of the active additive that contains grafted bioligands complementary to the cancer cells component. E.g. in [6] drug was delivered by the polylactide-based polymeric nanoparticles, synthesized by the emulsion polymerization, with grafted heptapeptide that is complementary to the cells of lung cancer. Studied cytotoxin was delivered to the targeted tumor with high selectivity. The disadvantage of this approach is the possibility of early toxin release and poisoning of healthy cells.

Corresponding author: E.G. Zemtsova, e-mail: ezimtsova@yandex.ru

© 2018 Advanced Study Center Co. Ltd.

2) The drugs should be encapsulated since they are toxic also for the cells of healthy tissues. Therefore, the drug should be isolated for the entire time of transportation. To do this, different approaches are used: e.g. in [6] the drug was grafted to the polymer. This approach is far from ideal because there is no continuous envelope covering the toxin. In work [6] the method of drug transport in liposomes with grafted bioligands was applied. This approach is very promising, since the drug is completely localized inside the liposome. However, there is no mechanism to deliver the drug exactly to the biological target. Another problem of this approach is related to the completeness of drug encapsulation, and its timely and rapid release into the tumor zone.

Another promising improvement of drug transport is the introduction of toxins into cells in bound form. So, it is possible [7] to use biomimetic method of cytotoxin doxorubicin delivery by means of transport in macrophages (cells of the immune system that move by the blood flow, with the size of 15-80 micrometers, capable of actively capturing and digesting bacteria, dead cell residues and other foreign or toxic particles). In this case, the toxin is localized in the cytoplasm of the transport cell, which excludes its release outside the tumor. It should be noted that here are also difficulties with the release (desorption) of the drug exactly in the biological target. Also, the disadvantage of this method includes the fact that lack of additional encapsulation of the drug can lead to the macrophage poisoning.

In this regard, synthesis of smart materials for targeted drug delivery with improved functional properties is an important task.

Our ongoing work on the RFBR grant [8,9] is devoted to the method of synthesis of a new smart material for targeted drug delivery, namely, the composite system *mesoporous silica (MCM-41)–magnetite nanoparticles (Fe_3O_4) or (Fe^0)–immune cells (macrophages)*. An important step in the development of smart material is the creation of a magnetic part of the composite system *mesoporous silica–magnetic nanoparticles*. This system will allow magnetic decapsulation (delivery) of medicals form the material (silica) using a magnetic field of a given value in the right place of the body.

In the present work, we studied the conditions of synthesis of magnetic nanoparticles Fe_3O_4 or (Fe^0) in MCM-41 silica pores Fe_3O_4@MCM-41 or (Fe^0)@MCM-41. This is the important stage of the production of smart material for controlled drug delivery. Magnetic structures optimized for pharmaceutical and biomedical needs must have very small size and narrow size distribution together with high magnetization values. In addition, these nanoparticles (NPs) must combine high magnetic susceptibility for optimal magnetic enrichment and loss of magnetization after magnetic field removal.

2. EXPERIMENTAL

2.1. Synthesis of mesoporous matrix MCM-41

Mesoporous MCM-41 matrix is synthesized by the condensation of tetraethoxysilane (TEOS) hydrolysis products [10,11]. Porosity of matrix is due to the specific steric conditions that formed in the medium of micellar surfactant template. Produced mesoporous material has pore diameter of ca. 35 Å, silica walls thickness between pores is ca.10 Å. As a result, the specific surface is as high as 1000 m^2/g. Primary silica structure is formed by means of self-assembly of inorganic component on the surfactant micelles surface. Common surfactants for silica synthesis have the general formula $C_nH_{2n+1}N(CH_3)_3Br$, with n=12–18. In polar solvent (in this case, water) surfactant consists of charged $[N(CH_3)_3]^+$ (hydrophilic head) and hydrophobic neutral part $[CH_3(CH_2)_{n-1}]$. In solution even at low concentrations, these ions form micelles with positively charged surface. So, surfactant micelles form hexagonal order in water. Inorganic component with the opposite charge adsorbs on the micellar surface and replaces surfactants' counterions. Being adsorbed on the surface as well as in intermicellar space, inorganic molecules form polymers by condensation reaction. Silica walls are formed from amorphous SiO_2 between the micelles. Subsequent removal of organics by the calcination at 600 °C results in free pores formation.

2.1.1. Standard synthesis of MCM-41

Mesoporous silica synthesized in two-necked flask using two-stage process. Firstly, micellar solution was obtained. Distilled water (170 ml), ethanol (60 ml), aqueous ammonia (43 ml), and CTAB (1.46 g) were mixed together using the mechanical stirrer during 30 minutes until homogenization. Afterwards, TEOS (4.6 ml) was added dropwise while stirring. As the result of the hydrolysis, orthosilicic acid was formed:

This unstable acid subsequently condensed to form the gel:

$$n\mathrm{Si(OH)_4} = (\mathrm{SiO_2})n\,[(\mathrm{H})]_2\mathrm{O})_{2n-m} = m\mathrm{H_2O}.$$

The as-obtained solution was aged for 2 h with stirring. After that, the resulting precipitate was fil-

tered out on the Buchner funnel. The sample in the crucible was placed in a muffle furnace and heat treated in the following mode: drying for 30 min at 200 °C, then 30 min at 250 °C. Subsequently, the sample heated up to 600 °C and calcined for 40 min at this temperature. After cooling to room temperature, the sample was carefully ground to avoid the globules aggregation.

2.1.2. MCM-41 synthesis using micellar expander 1,3,5-trimethylbenzene (TMB)

MCM-41 synthesized with minor difference compared to technique described in 2.1.1. Before TEOS, TMB (1:1 ratio to the surfactant) was added to the reaction. This material, being incorporated in surfactant micelles, leads to diameter increase i.e. acts as micellar expander. After TMB addition, reaction was mixed for 1.5 h. Subsequent operations were the same as in standard technique.

2.1.3. MCM-41 synthesis with the post-synthetic hydrothermal treatment (HTT)

Besides micellar expander we also used HTT to increase MCM-41 pore size diameter. Before filtration, the gel (MCM-41 filled with template), was autoclave-heated for 12 h at 120 °C. Subsequently, the solid was filtered and calcined analogously to standard technique.

In addition to micellar expander (section 2.1.2) and post-synthetic HTT (section 2.1.3) we also combined these two techniques: gel with the expander transferred to autoclave and high-temperature treated. After filtration, the sample was calcined analogously to standard technique.

2.1.4. Synthesis of MCM-41 with micellar expander TMB, co-expander (n-decane, $C_{10}H_{22}$) and TEOS hydrolysis catalyst (pyridine)

For further increase of MCM-41 pore size we additionally modified the standard technique described in the section 2.1.1. Here, we added n-decane as co-expander to the water-ethanol-ammonia-CTAB mixture. After 2 h stirring, TMB expander was added along with pyridine as the TEOS hydrolysis catalyst. Stirring was continued for further 2 h; after that TEOS was added. Further manipulations were analogous to the standard technique.

We prepared the series of samples with variation of n-decane/CTAB molar ratio (5:1, 11:1, and 17:1), at constant molar ratio TMB/CTAB (3:1). So, total micellar expander content was 8:1, 14:1, and 20:1, respectively. Pyridine amount was 0.1 wt.% of the mixture before TEOS addition.

2.2. Synthesis of magnetic nanoparticles in mesoporous silica matrix MCM-41

In mesoporous MCM-41 we synthesized nanoparticles of iron or magnetite. These substances exhibit positive magnetization in an external magnetic field. In addition, some regions of these particles may have non-zero magnetic moment in the absence of a magnetic field. This phenomenon is called spontaneous magnetization; in turn, Fe^0 NPs are ferromagnetic. In magnetite ($FeO{\cdot}Fe_2O_3$), iron ions form two sublattices with different magnetization. This indicates its ferrimagnetic nature. When size reached 5–10 nm, magnetite transforms to superparamagnetic state.

To get nanoparticles of iron or magnetite in MCM-41 pores, we introduced aqueous iron(III) chloride into initial matrices by the vacuum impregnation with subsequent reduction in the hydrogen stream until Fe^0 or Fe_3O_4.

2.2.1. Synthesis of iron nanoparticles in mesoporous MCM-41 silica matrix

A glass reactor for vacuum impregnation was used to introduce iron chloride into the silica matrix [12]. Initially, the sample was degassed in pentane by ultrasound. Then pentane was removed by drying in the oven at 150 °C. Then, the powder of the original matrix was placed in a glass reactor, hold in vacuum for 15 min, then aqueous iron chloride was poured into the reactor through the funnel. The liquid entering the surface of the grain is drawn into the pores due to the vacuum created at the previous step. The impregnated sample was placed in a Schott filter in order to remove excess of iron precursor from the MCM-41 grain surface. The sample was washed with methylene chloride until its color turns yellow. As-obtained samples contained iron chloride only in the pores. In order to get iron nanoparticles, samples were reduced in quartz reactor in the stream of dry hydrogen at 600 °C for 6 h. In order to protect iron from the oxidation by air, dry hydrogen stream was continued also at the sample removal.

2.2.2. Synthesis of magnetite nanoparticles in mesoporous MCM-41 silica matrix

Magnetite nanoparticles in mesoporous mesostructured matrix MCM-41 were synthesized similarly to the method described above. The time and the temperature of the reduction by dried hydrogen were different. Our experiments were performed at 330 °C during 6–9 h.

2.3. Analytical methods

X-ray analysis in this work was carried out at wavelength λ = 1.541 Å (CoK_α) using powder diffractometer Bruker "D2 Phaser". Small angle X-ray scattering (SAXS) is able to give direct information about the structure of matter and about the mutual distribution of scattering particles. In this work, SAXS measurements were done at X-ray wavelength λ = 1.541 Å (CoK_α) on the small angle diffractometer "SAXSess mc²". Adsorption studies of MCM-41 silica samples (calculation of specific surface area and pore diameter) were done on adsorption meter ASAP 2020 MP.

Iron content in the sample was detected using sulfosalicylic acid. In alkaline medium, this indicator forms a stable yellow complex with iron, which makes possible the photometric determination.

Particle size analysis performed using scanning electron microscope (SEM) Zeiss Supra 40P and by means of laser diffraction analyzer Mastersizer 3000. Phase composition and valence state of the samples were studied by Moessbauer spectroscopy with ^{57}Co source transformed into ^{57}Fe. Magnetic properties of the obtained particles were analyzed using vibromagnetometer Lake Shore 7410 in the fields from 0 to 1 T. In the course of measurements the saturation magnetization values and coercive force were determined.

3. RESULTS AND DISCUSSION

3.1. Synthesis of mesoporous silica MCM-41 and study of its structure.

The first step of this work was the synthesis of mesoporous silica matrix MCM-41, which was subsequently used as a nanoreactor for the synthesis of iron and magnetite nanoparticles in the matrix pores. Its structure has been analyzed by means of SAXS. SAXS pattern is depicted in Fig. 1. From the diffraction peak q = 1.704 nm^{-1}, where q is scattering vector, interplanar spacing of 36 Å was calculated using the formula q=2p/d.

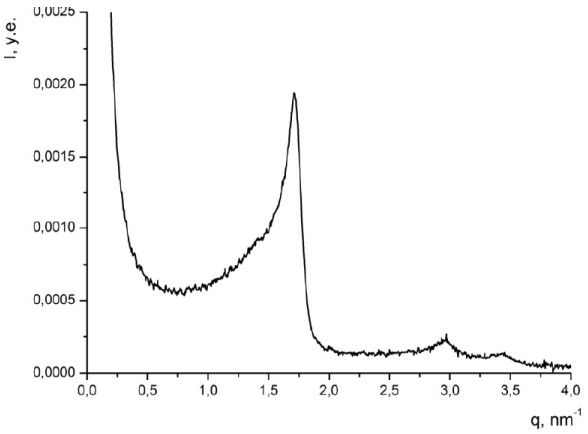

Fig. 1. Small angle X-Ray diffraction pattern of MCM-41.

During adsorption studies we experimentally obtained the adsorption isotherm of initial MCM-41.

The adsorption isotherm (not shown) is in accordance with the literature data for mesoporous objects and has a hysteresis loop associated with various adsorption and desorption mechanisms of the adsorbate. A differential pore size distribution curve was constructed based on the adsorption isotherm. The resulting curve had a maximum at the pore diameter of 33 Å. Pore volume for this sample was 0.87 cm^3/g. Similar measurements were made for all other MCM-41-based samples. According to SEM, particle size of mesoporous silica varies from 200 to 500 nm.

When TMB was used in 1:1 ratio to the template weight (MCM-41 No.2), interplanar spacing increased by 2 Å and reached 38 Å. The pore diameter calculated from the adsorption isotherm was 35 Å. Specific porosity increased from 0.87 cm^3/g to 0.91 cm^3/g, as expected.

Additionally, for increase of the pore diameter, we used post-synthetic autoclave treatment of the gel at 120 °C in different variations. Firstly, we performed autoclave heating (12 h at 120 C) of the sample synthesized using TMB (TMB/CTAB = 1:1). Here, we have obtained a distorted MCM-41 structure with bimodal pore distribution (adsorption data indicate two clear maxima at 28 Å and 39 Å), that can be explained by the incomplete TEOS hydrolysis. More likely, remaining TEOS hydrolyzed during HTT without formation of the ordered structure. To avoid the problem, we increased time of gel aging (from 2 to 24 h). Another solution to this problem was the addition of pyridine as the TEOS hydrolysis catalyst. According to the results of adsorption studies with

Table 1. Geometrical parameters of silica samples.

Sample	S_{BET}, m^2/g	V_{SP}, cm^3/g	d_{pores}, Å	d_{100}, Å	Expander used	Co-expander used
MCM-41 No.1	1105±55	0.87±0.026	33	36±1	-	-
MCM-41 No.2	1061±53	0.91±0.027	35	38±1	+	-
MCM-41 No.3	987±49	1.26±0.038	45	53±1	+	+
MCM-41 No.4	1012±51	1.71±0.051	49	67±1	+	+
MCM-41 No.5	1011±51	1.59±0.047	51	73±2	+	+

Table 2. Pore size and composition of the samples MCM-41/Fe.

Sample	d_{pores}, Å	ω Fe, %	ω Fe^0, %
MCM-41/Fe (No.1)	33	10.3±0.2	97
MCM-41/Fe (No.2)	35	12.2±0.3	96
MCM-41/Fe (No.3)	45	17.8±0.4	95
MCM-41/Fe (No.4)	49	23.5±0.5	96
MCM-41/Fe (No.5)	51	25.4±0.5	99

the pyridine addition, pores were increased by 7 Å comparing to the standard sample.

Since we could not get more suitable pore growth, it was decided to use expanders with co-expanders. As the co-expander we chose n-decane ($C_{10}H_{22}$). According to this technique, we obtained three samples with different molar ratio n-decane/CTAB (5:1, 11:1, and 17:1). Molar ratio TMB/CTAB was kept constant (3:1). Also, since the catalysis shows positive results, the remaining syntheses were carried out with pyridine. According to SAXS data, interplanar spacings for 5:1, 11:1, and 17:1 silica samples were 53, 67, 73 Å, respectively. Type IV adsorption isotherms of the samples is typical for mesoporous objects. Respective pore sizes were 45, 49, and 51 Å. With co-expander amount increase in the reaction mixture, we observe an expected increase in the interplanar distance and pore diameter of the resulting silica.

From synthesized MCM-41 matrices, five samples with increasing pore diameter was selected for further iron introduction. Table 1 shows the parameters of these silica samples.

3.2. Synthesis of Fe^0 nanoparticles in the pores of MCM-41

The next stage of work was the synthesis of Fe NPs in the pores of MCM-41. We used vacuum impregnation of the initial matrices by aqueous ferric chloride (50% from saturation concentration). To remove the iron precursor from the surface of the particles, we washed the sample with dried methylene chloride. Washed samples were reduced in the hydrogen stream at 600 °C for 6 hours.

The absence of Fe^0 NPs contamination on the MCM-41 grains surface confirmed using SEM. Further, to confirm the presence of metallic iron in the MCM-41 samples we analyzed their phase composition using Moessbauer spectroscopy and chemical analysis. The samples had a fraction of iron(II) and iron(III) compounds, but the main component was metallic iron. Moessbauer data indicate that the amount of metallic iron in the sample MCM-41 No.1 was ranged from 95% to 99%. The mass fraction of iron in the samples was found by a chemical analysis. Moessbauer spectroscopy and chemical analysis data are presented in Table 2. Thus, the total iron content in the samples depends on the pore diameter.

With a decrease in the pore diameter, as can be seen, the proportion of iron in the samples decreased (Table 2).

Also, to confirm the presence of iron, the samples were examined using X-ray diffraction (Table 3). According to XRD, metallic iron amount in the samples ranged from 95% to 98%.

3.2.2. Synthesis of magnetite nanoparticles in MCM-41 pores

The next stage of work is the synthesis of magnetite nanoparticles in MCM 41 pores. Here we also used the method of vacuum impregnation of the silica

Table 3. Iron content in the samples (XRD data).

Sample	ω Fe^0, %
MCM-41/Fe (No.1)	98
MCM-41/Fe (No.2)	97
MCM-41/Fe (No.3)	96
MCM-41/Fe (No.4)	95
MCM-41/Fe (No.5)	98

matrix. Initially, in order to obtain magnetite, we impregnated the matrix with an aqueous solution of iron chlorides:

$FeCl_2 + 2FeCl_3 + 4H_2O = Fe_2O_3 + 8HCl$.

The sample was washed from chlorides by dry dichloromethane. Then the sample was purged by the gaseous ammonia. Synthesis of magnetite is failed because it was oxidized until α-Fe_2O_3. Magnetization curve confirms compound's paramagnetism.

Magnetite was synthesized using the technique, based on the vacuum MCM-41 impregnation by $FeCl_3$ solution, with subsequent reduction in the quartz reactor in the hydrogen stream at 330 °C for 8 h. As a result, we synthesized pure magnetite in the pores of MCM-41. Magnetite-containing samples were characterized using Moessbauer spectroscopy. However, it is known that Moessbauer spectrum and its parameters can significantly change during the transition of the sample to a single-domain and superparamagnetic state. E.g., in [45] the dependence of the Moessbauer spectrum shape on the particle size and the spectrum recording conditions is shown. Low temperatures studies revealed the fine structure, but despite the significant difference in the shape of the spectrum, recorded at 300K, its displacement can be used to evaluate the presence of magnetite. The Moessbauer parameters of MCM-41/Fe_3O_4 (Table 4) suggest that iron atoms exist in three states. The spectrum itself has three explicit doublets, one of which is poorly resolved, but in general, based on indirect grounds, the spectrum can be characterized as not resolved sextet.

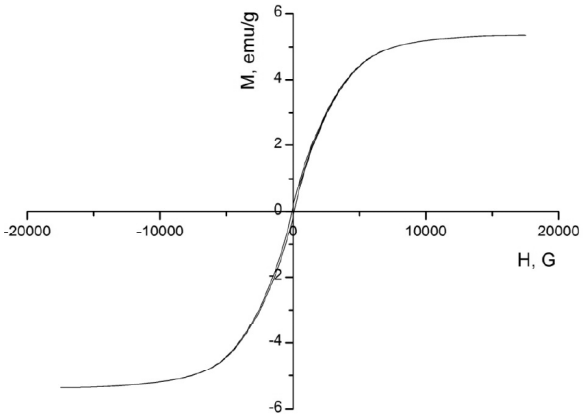

Fig. 2. Magnetization diagram for MCM-41/ Fe (sample No.1).

Chemical analysis of MCM-41/Fe_3O_4 gives magnetite content in the pores 8.75% and 10.5% for two samples (Table 5). There is three phase components in the spectrum. Main phase is magnetite, and in this case, splitting into a sextet is not observed due to the small particle size.

3.3. Investigation of magnetic characteristics of the samples

3.3.1. Magnetic properties of MCM-41/ Fe^0 samples

Magnetic properties of the samples were investigated using vibromagnetometer Lake Shore 7410 at 300K and 77 Hz. For evaluation of magnetic properties we used saturation magnetization value. Magnetization curve of the standard MCM-41/Fe is depicted on the Fig. 2. Magnetization curves for all the samples saturate smoothly; there is no hysteresis loop. This suggests that the samples are superparamagnetic.

Table 4. Moessbauer data for the sample MCM-41/ Fe_3O_4.

No. *	Doublets *G* (mm/s)	*IS* (mm/s)	*QS* (mm/s)	*S***, %
1	0.57±0.03	0.33±0.1	0.60±0.02	56.54
2	0.39±0.00	0.11±0.06	1.06±0.13	5.07
3	0.30±0.64	0.24±0.08	8.82±0.00	38.39

* Number refers to the state of iron in the MSM-41/ Fe_3O_4 sample.

** *S*- the calculated value characterizing the amount of iron in a certain state.

Table 5. Chemical composition of synthesized MCM-41/Fe_3O_4.

Sample	d_{pores}, Å	ω Fe_3O_4, %
No.1 MCM-41/Fe_3O_4	33	8.75±0.2
No.2 MCM-41/Fe_3O_4	45	10.5±0.2

Table 6. Magnetic properties of the studied nanocomposites MCM-41/Fe.

Sample	d_{pores}, Å	M_S, Am²/kg
MCM-41/Fe (No.1)	33	5.3±0.1
MCM-41/Fe (No.2)	35	10.8±0.1
MCM-41/Fe (No.3)	45	27.4±0.3
MCM-41/Fe (No.4)	49	38.8±0.4
MCM-41/Fe (No.5)	51	45.8±0.5

Our data indicate an increase of the saturation magnetization with the pore radius of matrix used for the synthesis. Table 6 displays the values of saturation magnetization of the samples containing iron nanoparticles and pore diameters of the corresponding silica matrices. Fig.3 depicts the linear increase of saturation magnetization value with the growth of the pore diameter of used MCM-41.

3.3.2. Magnetic properties of the samples MCM-41/Fe_3O_4

We also investigated the magnetic properties of the samples with magnetite nanoparticles embedded into mesoporous MCM-41. Two samples were synthesized using matrices with pore sizes of 33 and 45 Å. In Fig. 4, magnetization curve for the first nanocomposite is given. In Table 7, saturation magnetization values are given for MCM-41/Fe_3O_4 samples, together with specific magnetization calculated from the weight ratio in the samples. Maximal values of the specific magnetization are 84.6 Am²/kg and 82.8 Am²/kg, respectively, that is close to the value for pure magnetite (92 Am²/kg).

These values confirm the data for our magnetite. The curves saturate smoothly. However, hysteresis

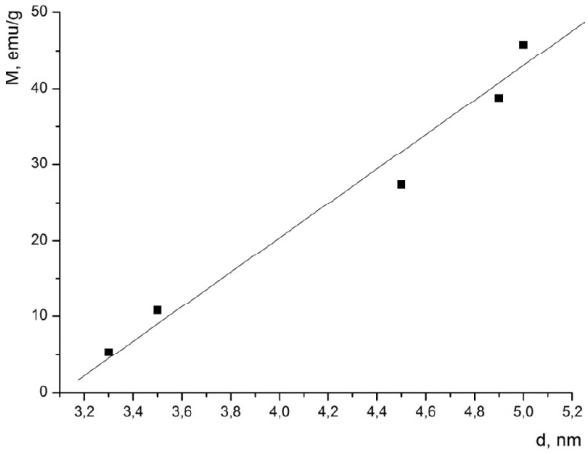

Fig. 3. The dependence of saturation magnetization of MCM-41/Fe on the matrix pores diameter (d).

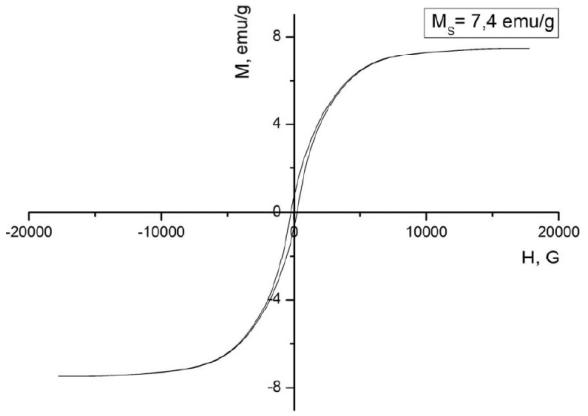

Fig. 4. Magnetization diagram for MCM-41/Fe_3O_4 (sample No. 1).

loop is present with a negligible quadratic coefficient. This curve does not correspond neither to superparamagnetic, nor to ferromagnetic state. Most probably such a shape is the result of the inclusion of ferromagnetic into superparamagnetic phase. Such inclusions could be explained by the formation of anisotropic magnetite particles during the soft reduction by the hydrogen.

4. CONCLUSIONS

In conclusion, we developed the synthetic procedures for mesoporous MCM-41 with various pore diameter (33-51 Å) and for superparamagnetic mag-

Table 7. Magnetic properties of MCM-41/Fe_3O_4 nanocomposites.

Sample	d_{pores}, Å	M_S, Am²/kg	M_{SP}, Am²/kg
MCM-41/Fe_3O_4 (No.1)	33	7.4±0.1	84.6±0.8
MCM-41/Fe_3O_4 (No.2)	45	8.7±0.1	82.8±0.8

netite or iron nanoparticles in the pores of mesoporous MCM-41. The dependence of the magnetic properties of MCM-41/Fe^0 and MCM-41/Fe_3O_4 on the pore radius of silica MCM-41 is studied. We found that the matrix has a decisive influence on the properties of the obtained nanomaterials, namely, on content of iron and magnetite nanoparticles. The saturation magnetization increases with the increase of matrix pores. We showed that nanocomposites MCM-41/Fe^0 and MCM-41/Fe_3O_4 demonstrate superparamagnetic behavior that makes it possible to use them as the magnetic material for the target drug delivery.

The research was carried out on the basis of the Resource centers "Innovative technologies of composite nanomaterials", "X-ray Diffraction methods of research", Educational resource center in the field of "Chemistry", Interdisciplinary resource center in the field of "Nanotechnology" of St. Petersburg state University.

ACKNOWLEDGEMENTS

The work is executed at financial support of Russian Foundation for basic research (grant No. 17-03-01331a).

REFERENCES

[1] V.M. Smirnov // *Russ. J. Gen. Chem*. **72** (2002) 590.

[2] J.-M. Lehn, *Supramolecular Chemistry, Concepts and Perspectives* (Weinheim, 1995).

[3] *Smart Materials,* ed. by Mel Schwartz (CRC *Press,* 2008).

[4] Wang Zhong-Lin and Z.C. Kang, *Functional and Smart Materials* (New York: Springer-Verlag New York Inc., 2013).

[5] *L*. H. Reddy, J. L. Arias and J. Nicolas Couvreur // *Chem. Rev.* **112** (2012) 5818.

[6] Yao Jiang // *Journal of Controlled Release* **221** (2016) 26.

[7] Kazuaki Ninomiya // *Ultrasonics Sonochemistry* **28** (2016) 54.

[8] E.G. Zemtsova, A.N. Ponomareva, V.V. Panchuk, L.F. Galiullina and V.M. Smirnov // *Reviews on Advanced Materials Science* **52** (2017) 82.

[9] E.G. Zemtsova, A.N. Ponomareva, P.E. Morozov, V.V.Panchuk, V.G.Semenov and V.M. Smirnov // *Russian Journal of General Chemistry* **85** (2015) 1973.

[10] E.G. Zemtsova, A.Y. Arbenin, A.F. Plotnikov and V.M. Smirnov // *Journal of Vacuum Science and Technology A: Vacuum, Surfaces and Films* **33** (2015), article 021519.

[11] E.G. Zemtsova, A.N. Ponomareva, P.E. Morozov, V.V.Panchuk, V.G.Semenov and V.M. Smirnov // *Russian Journal of General Chemistry* **85** (2015) 1973.

[12] M.A. Shevtsov, M.A. Parr, V.A. Ryzhov, E.G. Zemtsova, A.Yu. Arbenin, A.N. Ponomareva, V.M. Smirnov and G.Multhoff // *Scientific Reports* **6** (2016), article 29247.